Phase-Separation of Cellulose from Ionic Liquid upon Cooling: Preparation of Microsized Particles

Jingwen Xia
University of Helsinki: Helsingin Yliopisto
Alistair W. T. King
University of Helsinki: Helsingin Yliopisto
Ilkka Kilpelainen (✉ Ilkka.kilpelainen@helsinki.fi)
University of Helsinki https://orcid.org/0000-0001-8582-2174
Vladimir Aseyev
University of Helsinki: Helsingin Yliopisto

Research Article

Keywords: cellulose regeneration, spherulite, UCST, phosphonium acetate

Posted Date: May 10th, 2021

DOI: https://doi.org/10.21203/rs.3.rs-468251/v1

Abstract

Cellulose is an historical polymer, for which its processing possibilities have been limited by the absence of a melting point and insolubility in all non-derivatizing molecular solvents. More recently, ionic liquids (ILs) have been used for cellulose dissolution and regeneration, for example, in the development of textile fiber spinning processes. In some cases, organic electrolyte solutions (OESs), that are binary mixtures of an ionic liquid and a polar aprotic co-solvent, can show even better technical dissolution capacities for cellulose than the pure ILs. Herein we use OESs consisting of two tetraalkylphosphonium acetate ILs and dimethyl sulfoxide (DMSO) or γ-valerolactone (GVL), as co-solvents. Cellulose can be first dissolved in these OESs at 120°C and then regenerated, upon cooling, leading to micro and macro phase-separation. This phenomenon much resembles the upper-critical solution temperature (UCST) type thermodynamic transition. This observed UCST-like behavior of these systems allows for the controlled regeneration of cellulose into colloidal dispersions of spherical microscale particles (spherulites), with highly ordered shape and size. While this phenomenon has been reported for other IL and NMMO-based systems, the mechanisms and phase-behavior have not been well defined. The particles are obtained below the phase-separation temperature as a result of controlled multi-molecular association. The regeneration process is a consequence of multi-parameter interdependence, where the polymer characteristics, OES composition, temperature, cooling rate and time all play their roles. The influence of the experimental conditions, cellulose concentration and the effect of time on regeneration of cellulose in the form of preferential gel or particles is discussed.

Regular micro-sized particles regenerated from a cellulose-OES mixture of tetrabutylphosphonium acetate:DMSO (70:30 w/w) upon cooling.

Introduction

Cellulose is widely used in various industries and material processing, although it has not reached the same scale of use, compared to petrochemical-based polymers, as it lacks a melting point and does not dissolve in any non-derivatizing molecular solvents. More modern applications, involving dissolution and regeneration, include regeneration and spinning into textile fibers. This is already commercialized using NMMO-water mixtures, in the form of the Lyocell process (Fink *et al*. 2001). In many of these applications, pre-dissolution of cellulose, to form close to isotropic solutions, is assumed. Cellulose has a very low solubility in water and other conventional organic solvents because of the extensive H-bonding network and amphiphilicity of the rigid cellulose chains. Therefore basic-amphiphilic solvents, such as ILs, have been successful in the dissolution of cellulose.(Himmel *et al*. 2007; Nishiyama *et al*. 2003) Ionic liquids (ILs) were first demonstrated to dissolve cellulose by Swatloski *et al*. in 2002 (Swatloski *et al*. 2002). ILs are salts, typically composed of an organic cation and an inorganic or organic counter anion. They often possess high thermal and chemical stability, although the cellulose-solvating structures tend to be the least stable (King *et al*. 2012). Several types of ILs that can be used in cellulose dissolution have been reported, *e.g*. ILs based on imidazolium, ammonium and phosphonium cations (Clough 2017). Anions are always basic, such as chloride and acetate. While the dissolution of cellulose in ILs has already been

investigated to a good extent, the regeneration processes can be highly complex (Hauru *et al*. 2016) and vary from application to application.

One of the most attractive applications using ILs, due to its relative simplicity, is the IONCELL process (Sixta *et al*. 2015). This is an air-gap (dry-jet wet) spinning process where cellulose is dissolved in IL and drawn from a spinneret in an air-gap and then into a water bath. The shear forces from the spinneret and draw orient the cellulose polymer into a state which allows for rapid regeneration into parallel cellulose II crystallites. This imparts high strength to the fibers when stressed along the fiber axis. The final cellulose regeneration, to cellulose II, takes place during the IL washing and fiber drying stages. There are some early examples of using traditional imidazolium based ILs in air-gap spinning (Ingildeev *et al.* 2013; Sixta *et al*. 2016). However, their inherent reactivity towards cellulose and instability, (King *et al*. 2012; Schrems *et al.* 2010) in general, presents difficulties in efficient solvent recycling and minimization of cellulose degradation. Recent advances in synthesis of recyclable ILs, like distillable superbase carboxylate ILs used in the IONCELL process, have resulted in scaling up towards industrial production (Elsayed *et al*. 2020a; Elsayed *et al.* 2020b; Hauru *et al.* 2016; King *et al.* 2011; Parviainen *et al.* 2013; Sixta *et al.* 2015). In general, these superbase-derived ILs have lower thermal and chemical stabilities yet find application. On the opposite of the stability scale, tetraalkylphosphonium-based ILs are among the most stable ILs, both thermally and chemically. They are known to dissolve cellulose as the OESs (Holding 2016; Holding *et al.* 2017) and are even applied as solvents for solution-state NMR analysis of crystalline celluloses (King *et al.* 2018; Koso *et al.* 2020) at high dilution in DMSO-d_6.

Aside from their high cost, tetraalkylphosphonium ILs offer interesting potential for cellulose processing, over the different phase-compositions of IL and co-solvent (Rico del Cerro *et al*. 2020). Pure tetraalkylphosphonium acetates do not dissolve cellulose, as such, but become excellent solvents if mixed with a polar aprotic co-solvent, e.g. dimethyl sulfoxide (DMSO) or γ-valerolactone (GVL) These binary mixtures, so called organic electrolyte solutions (OESs), have lower viscosities and readily dissolve cellulose in high concentrations, which may be beneficial for a range of applications (Clough 2017; Clough *et al.* 2017; de Oliveira *et al.* 2016; Parviainen *et al.* 2013; Rinaldi 2011). Naturally, the solvation properties of OESs also differ from those of the pure ILs, which alters the thermodynamic and kinetic balance of competing factors, *e.g.* ion-pair separation, bonding interactions, mass transport *etc*.. This picture is not yet totally clear in the literature. However, there are now several studies demonstrating novel phase-behavior by varying regeneration conditions.

The solution crystallization of spherulitic microparticles of cellulose has been observed previously for *N*MMO-water solutions (Chanzy *et al*. 1979; Roy *et al.* 1984). A similar phenomenon has been observed for the ILs (Song *et al.* 2013). It has also been observed that the phase-separation of cellulose happens in the mixture of 1-ethyl-3-methylimidazolium acetate with 1,3-dimethyl-2-imidazolidinone ([C_2C_1im][OAc]:DMI), upon cooling below the cloud point temperature (T_{cp}) (de Oliveira *et al.* 2016). This phenomenon resembles the upper critical solution temperature behavior (UCST), known for synthetic polymers. However, exact nature of this separation in the cellulose-OESs systems and overall understanding of its solution thermodynamics is still underway. Two recent articles suggest the

crystallization of a cellulose-ionic liquid complex, during spherulite formation. (Song *et al.* 2018; Nishiyama *et al.*2003). In spite of the better dissolution capacity of tetrabutylphosphonium acetate based OESs, in comparison to pure IL, the range of concentration where cellulose forms relatively isotropic solutions, in OESs, is narrow (Holding *et al.* 2017). Using the UCST-type phenomenon for crystallization of particles from a synthetic polymer melt, has already been suggested (Arnauts and Berghmans 1987; Callister *et al*. 1990; Willcock *et al.* 2014). However, the complexities in recovering usable particles from OESs requires further work.

In this paper, we use two separate tetraalkylphosphonium acetate ILs as components of OESs for dissolution of the microcrystalline cellulose (MCC). We study this UCST-type phase-separation behavior for regeneration of cellulose, in a controllable fashion. Due to their good thermal and chemical stabilities, (Bradaric *et al*. 2003) and relatively low IL toxicities (Mikkola *et al.* 2015), we use tetrabutylphosphonium acetate ($[P_{4444}][OAc]$) and methyltributylphosphonium acetate ($[P_{4441}][OAc]$), see Figure 1. The length of the alkyl chain in the cation influences the toxicity: the longer alkyl chains make ILs more toxic. However, the short-chained $[P_{4444}][OAc]$ and $[P_{4441}][OAc]$ cannot directly dissolve cellulose. Therefore, co-solvents are added, Figure 2 and the phase-behavior studied.

Experimental

Materials

Microcrystalline cellulose (MCC, Avicel® PH-101) was purchased from Sigma-Aldrich and oven-dried at 60 °C for 18 h, before dissolution. $[P_{4441}][OAc]$ was synthesized by reaction of acetic acid with tributyl(methyl)phosphonium methylcarbonate (70 wt.% in methanol, IoLiTec GmbH, Heilbronn, Germany) as described in Supplementary information (SI). $[P_{4444}][OAc]$ (> 95%, IoLiTec GmbH, Heilbronn, Germany) was dried under vacuum at 80 °C for 5 h, with slow turning of the mixture. The final water contents of these ILs were measured using Karl-Fischer titration, to be below 0.5 wt.%. Dimethyl sulfoxide (DMSO, > 99.98% Fischer Chemicals, Finland) was stored over pre-dried 3 Å molecular sieves, to avoid water absorption. The following chemicals were used as purchased: 1,3-dimethyl-2-imidazolidinone (DMI, >99.0%, TCI Europe, Belgium), 1,3-dimethyl-3,4,5,6-tetrahydro-2(1H)-pyrimidinone (DMPU, >98.0%, TCI Europe, Belgium), acetic acid (AcOH, >99.8%, Sigma-Aldrich, Finland), γ-valerolactone (GVL, >99.0%, Sigma-Aldrich, Finland), acetone (>99.0%, Sigma-Aldrich, Finland), isopropyl alcohol (IPA, >99.0%, HoneyWell, Germany), chloroform (>99.0%, HoneyWell, Germany), methanol (MeOH, >99.99%, Fischer Chemicals, Finland).

Procedure for measurement of the cellulose dissolution capacity of $[P_{4444}][OAc]$-co-solvent compositionsat 120 °C (5 min mixing of aliquots)

Binary OESs containing $[P_{4444}][OAc]$ as an IL-component (see Figure 1) and DMSO, GVL, DMI or DMPU as co-solvents (see Figure 1) were prepared between 10:90 and 90:10 w/w with a composition interval step of +10/-10. An initial 15 mg of MCC was added to 3.0 g of OES upon continuous mixing at 20 °C and

then heated up to 120 °C. The 'saturation limit' was determined by subsequent addition of MCC in 15 mg aliquots, at 120 °C. After each addition, solution was agitated for 5 min to dissolve the added MCC. Magnetic stirring was used when the concentration of cellulose was relatively low. More concentrated solutions were too viscous, and the solutions were mixed manually with a stainless-steel spatula. Turning of the sample was minimized, to avoid the formation of air bubbles. When the saturation point was reached, further aliquot additions resulted in opaque solutions, after 5 min of mixing. The saturation point was estimated as mid-point between the concentration of the opaque solution and that of the preceding clear solution. Note that if the concentrated cellulose solutions are subjected to long dissolution times (> 8 minutes) at 120 °C, this sometimes results in darker mixtures. This color is likely due to formation of trace amounts of intense chromophores from residual pentose degradation. However, it does not seem to affect the studied regeneration phenomena.

Dissolution of MCC for regeneration phase diagram preparation

Our experiments suggest that OESs containing DMSO have much higher dissolution capability for MCC than that of OESs containing GVL. For comparison of phase-behavior of these OESs, the IL:DMSO or IL:GVL composition was chosen to be 70:30 w/w. To prepare the solutions, MCC powder was first dispersed in OESs at room temperature (RT), then heated up to 60 °C for 40 min, to initially swell the crystallites, and finally heated up to 120 °C for 5 minutes, for complete dissolution. The color of the cellulose solutions slightly changes during dissolution from light yellow to yellowish-orange and may even become darker, if the time of dissolution at 120 °C is prolonged. The enthalpy of the dissolution process was examined by means of differential scanning calorimetry (DSC, *DSC Q2000, TA instrument*), using 5.0 wt.% solutions of cellulose in $[P_{4444}][OAc]$:DMSO. DSC suggests that complete dissolution occurs above 90 °C and the details are shown in the SI. An *Olympus microscope BX 51* was used to confirm complete dissolution: no undissolved MCC material was observed under the optical microscope. The phase diagram for the separation of cellulose, upon cooling from $[P_{4444}][OAc]$:DMSO, was successfully obtained for the concentration range between 2.0 and 9.0 wt.%. Regeneration of cellulose in the form of particles was mainly studied using solutions of 2.0 wt.% in $[P_{4444}][OAc]$:DMSO and 5.0 wt.% in $[P_{4441}][OAc]$:DMSO.

Observation of the phase-separation phenomenon

The cloud point temperature (T_{cp}) defined the phase-separation boundary, upon cooling the cellulose solutions. T_{cp} was detected by means of transmittance measurements using a *Jasco V-750* UV-Vis spectrophotometer. Quartz cuvettes with path-length of 10mm (*Hellma Analytics*), polished on two sides were used. The UV-spectrometer was baseline corrected with distilled water at RT and then heated to 90 °C, prior to the measurements. 2 ml MCC solutions were prepared in the UV cuvettes, the cuvettes were sealed with Teflon tape after filling of solutions, at 120 °C - described above, and quickly transferred to the UV-spectrometer. These were then equilibrated at a cuvette temperature of 90 °C for 10 min. Transmittance was measured with a cooling rate of set 1 °C/min in the range of 90-20 °C, at a wavelength of 600 nm (out of the range of UV-absorbing chromophors). The intensity of light scattered at

the 173 ° angle (*ZetaSizer Nano, Malvern Instruments*) was used to follow the phase transition on the micro to nano particle scale (see the SI). Examples of rheological studies (*Discovery HR-2 Hybrid Rheometer, TA Instrument*), where appropriate, are also given in the SI.

Regeneration of cellulose upon cooling

Depending on the experimental conditions, cellulose regenerates in the form of either spherical particles, multi-particle clusters or as macroscopic gel. Freshly prepared solutions (3 g in 20 ml vial) were cooled from 120 °C down to and below T_{cp}, using the same cooling procedure - unless stated otherwise. In accordance with our standard cooling conditions, cellulose solutions in $[P_{4444}][OAc]$:DMSO (70:30 w/w)were cooled down to room temperature (RT) in a fume hood and equilibrated for 18 h. In this case, the solution is cooled by the surrounding air, without additional temperature control. Agitation of the solutions must be avoided to ensure sustained particle growth, in a stable environment. This regeneration process typically results in micro-sized spherical particles for solutions of 1-3 wt.% concentration. Formation of particles in solutions of 0.5 wt.% and below was not detected. Increasing cellulose concentration over 4 wt.% promotes a more homogeneous macro gel-formation. Similar experiments were made on cellulose solutions in $[P_{4441}][OAc]$:DMSO or GVL and the results are shown in the SI. An Optical microscopy (*Olympus microscope BX 51*) was used for observing the regenerated cellulose after equilibration as well as for visualization of the particle growth. Smaller particles were studied by means of dynamic light scattering (*ZetaSizer Nano, Malvern Instruments*).

Recovery of the cellulose from the OELs

1-2 wt.% solutions (3 g in a 20 ml vial) in$[P_{4444}][OAc]$:DMSO (70:30 w/w) were the most successful for regeneration of cellulose, in the form of spherical particles. Once the particles were formed, $[P_{4444}]$ [OAc]:DMSO was exchanged with water: 10 times the volume of water was added into the mixtures and sonicated for 20 min (*UP100Hprobe ultrasound processor*, *Hielscher*). The particles in the aqueous mixture were sedimented using an *Eppendorf 5810 R Centrifuge* (3000 rpm for 20 min at RT). The centrifugation was repeated 3 times to ensure complete removal of $[P_{4444}][OAc]$ and DMSO. The precipitates, after the last washing, were freeze-dried (*Heto Maxi Dry Lyo Freeze-dryer*). The crystalline phase-composition and the approximate content of the amorphous phase in the regenerated cellulose were determined my means of wide-angle X-ray scattering (WAXS) measurements, performed on a *PANalytical X'Pert Pro MPD* system. The diffracted intensity of Cu Kα radiation (λ = 1.54 Å, 45 kV, 40 mA) was measured over a 2θ-angular range between 5° and 50°; 50 mg of the dried product was pressed to a 10 mm diameter disc, in an IR press, for measurement using Bragg-Brentano (reflection) geometry, on a glass plate. Crystallinity was determined by Pseudo Voigt peak, amorphous background and glass background fitting, using *Fityk (Wojdyr 2010)*, as published previously (Rico del Cerro *et al*. 2020).

Results And Discussion

Effect of co-solvent on dissolution of cellulose in $[P_{4444}][OAc]$-based OESs

The dissolution power of binary OESs containing $[P_{4441}][OAc]$ or $[P_{4444}][OAc]$ strongly depends on the co-solvent selection. In order to choose a proper co-solvent for cellulose dissolution and regeneration, the dissolution capacity of cellulose in various OESs compositions containing DMSO, GVL, DMI and DMPU (see Figure 1), was determined and the results are presented in Figure 2.

As is seen in Figure 2, $[P_{4444}][OAc]$:DMSO has the highest dissolution ability, whereas the ability of $[P_{4444}][OAc]$:GVL to dissolve cellulose is the poorest. OESs containing DMPU and DMI have almost the same dissolution capacity for cellulose except the range of compositions where cellulose will start to dissolve is ~ 30 wt.% co-solvent. It is well understood that cellulose will dissolve if the anions of the IL can form strong hydrogen-bonds with the hydroxyl groups of cellulose (Andanson *et al.* 2014; Rabideau *etal*. 2013; Rabideau *et al.* 2014). There is the proposal that the lower viscosities of the OES solutions lead to faster kinetics of cellulose dissolution, without any increase in ionicity leading contributing to the dissolution capability (Andanson *et al.* 2014). However, Huo *et al.* (Huo *et al.* 2013) have demonstrated an enhancement in the interaction of chloride ions with cellulose, at high DMSO compositions of the [bmim]Cl:DMSO system, using molecular dynamics. Not surprisingly water, as co-solvent, was shown to significantly weaker this interaction. This suggests that the co-solvents that are stronger dipolar aprotic solvents are more likely to improve the dissolution of cellulose. Therefore, the polarity of the aprotic co-solvent is a determining factor that may influence the OESs dissolution capacity. Using the dipole moment (D) of polar aprotic solvents (Lopez *et al.* 2018), we get the order of co-solvent in respect to their polarity: DMSO (0.444 D) > DMPU (0.352 D) > DMI (0.325 D) > GVL (0.302 D). This polarity order is in a perfect agreement with the order of dissolution capacities presented in Figure 2.

From the dissolution efficiency viewpoint, DMSO is the best performing co-solvent among those studied. As is shown in Figure 2, the highest saturation concentration of 17.3 wt.% is obtained, when the OESs contains 60 wt.% of $[P_{4444}][OAc]$ and 40 wt.% of DMSO. Our earlier studies suggest that $[P_{4441}][OAc]$:DMSO demonstrates a similar trend in dissolution capacity as for $[P_{4444}][OAc]$:DMSO (Holding 2016; Holding *et al.* 2014).

Owing to the higher dissolution capacity, OESs containing DMSO provide a broader phase dissolution range. However, $[P_{4444}][OAc]$:DMSO (60:40 w/w) with the highest dissolution capacity does not yield particles of a regular shape upon cooling (see Figure S3, S4 in SI). One may say that when the dissolution capability of OESs is high, thermodynamic quality of the solvent is “too good” and more cellulose can be dissolved in such a solvent. A high degree of cellulose swelling at elevated temperature (in a good solvent), and possibilities for higher solution saturation concentrations unfortunately favor regeneration of cellulose in the gel form, upon cooling. On the other hand, if we decrease the cellulose concentration in a system, with high dissolution capacity, no phase-separation is observed in the practical range of temperatures (20-60 °C) as the solvent quality is simply “too good”. In other words, the dissolution capacity of OESs cannot be too high if we want to observe phase-separation in this practical range.

Our preliminary experiments suggested that the best particles, with uniform shape and size, are obtained in $[P_{4444}][OAc]$:DMSO (70:30 w/w). For comparison, particles obtained in $[P_{4444}][OAc]$:DMSO (65:35 w/w)

and $[P_{4444}][OAc]$:DMSO (75:25 w/w) are shown in SI (Figure S5, S6). Therefore, the $[P_{4444}][OAc]$:DMSO (70:30 w/w) composition was selected for further investigations to study the UCST-type phase transition and the regeneration of preferably spherical particles. Regrettably, DMSO is challenging for any large-scale production, due to its properties as a biological solvent and the low volatility which may pose difficulties in recycling of the OES components. In this respect, GVL is still a viable candidate due to lower hazards associated with this solvent, despite its lower dissolution capacity. The removal/recovery of GVL is straightforward, for example, with vacuum distillation. Therefore, $[P_{4444}][OAc]$:GVL (70:30 w/w) composition was studies as a reference. One needs to take into account that the dissolution capacity of cellulose in this OES is quite low, which gives a very narrow window of solution concentrations for the phase-separation and regeneration experiments (see Figure S7).

Phase-separation and the phase diagram

A classic example of UCST-type behavior in polymer chemistry is that of polystyrene in cyclohexane (Sun *et al.* 1980; Swislow *et al.* 1980). The solubility of polystyrene changes upon decreasing temperature: cyclohexane is a good solvent at elevated temperature and turns poor upon cooling. Accordingly, T_{cp} is the temperature below the q-temperature where the phase-separation starts. Thus, it can be said that the thermodynamic quality of cyclohexane, as a solvent, is poor below T_{cp}. Below this temperature, individual polystyrene coils collapse and aggregate, resulting in phase-separation on a microscopic scale, the solution becomes opaque, milky and eventually polystyrene precipitates, in the course of this macroscopic phase-separation. This type of thermodynamic transition can be graphically described as a phase diagram, where T_{cp} is plotted *vs.* the polymer mass fraction, and presents the phase-separation boundary. T_{cp} is determined using turbidity measurements, light scattering or even with a naked eye.

Under certain experimental conditions, complete precipitation of polymers below T_{cp} does not occur and their aggregates remain colloidally stable (Arnauts and Berghmans 1987; Callister *et al.* 1990). As has been shown, multi molecular particles of synthetic polymers are spherical and dense in poor solvents. Interaction between them is elastic, which is explained by the viscoelastic effect and partial vitrification of polymeric material (Aseyev *et al.* 2006; Zhang and Wu 2006). Studies on such aggregates are typically performed using solutions with concentration below 0.01 wt.%, to decrease the number of inter particle collisions. Use of a viscous solvent, dioctyl phthalate, was also suggested to slow down the macroscopic phase-separation of polystyrene, upon cooling, which allowed for studies on more concentrated solutions (Stepanek *et al.* 1982). In contrast, the phase-separation behavior of cellulose in OESs, upon cooling, has not been investigated in such detail.

The UCST behavior of polystyrene in cyclohexane originates from the balance mainly weaker van der Waals interactions, allowing access to various conformers at specific thermal energies, *kT.* On the molecular level, this results in the coil-to-globule transition upon cooling. In contrast to this classical case, interactions in the cellulose-OESs include the much stronger long-range electrostatic interactions between charges, dipoles and hydrogen-bonding, in addition to the short-range van der Waals interactions. Presence of the co-solvent makes the interpretation even more complex. Moreover, cellulose is a semi-

flexible linear molecule and its folding is limited. Lowering the *kT* energy should favor the inter chain attraction, H-bonding and gradual crystallization. Furthermore, viscosity of the OES drastically increases with decreasing temperature, which significantly slows down mobility of cellulose chains similar, somewhat analogous to polystyrene in dioctyl phthalate (Stepanek *et al*. 1982). The slow dynamics suggests that the cooling rate and the cooling profile, together with the cellulose concentration, play key roles in the controlled cellulose regeneration.

Therefore and in accordance with the concepts discussed above, we built a phase-diagram for the UCST-type phase transition of cellulose in $[P_{4444}][OAc]$:DMSO (70:30 w/w). High dissolution capacity of this OESs, at 120 °C, suggests thermodynamically good conditions for cellulose dissolution and chains are expected to become highly solvated and loosely interacting. Thermodynamic quality becomes poorer with decreasing temperature, similar to polystyrene in cyclohexane (Sun *et al*. 1980; Swislow *et al.* 1980) or in dioctyl phthalate (Stepanek *et al.* 1982). Individual cellulose chains gradually lose their solubility. Inter and intramolecular interactions become more persistent. Below a certain temperature (assuming q-conditions in the vicinity of T_{cp}), these chains extensively associate, their aggregates become denser and larger with time and eventually form micro-sized particles, that can be detected with an optical microscope. The particles make the solutions opaque and cloudy, which allows for turbidity measurements.

Figure 3 presents results obtained from the cellulose solution in $[P_{4444}][OAc]$:DMSO (70:30 w/w) with a constant cooling rate of 1 °C/min. For example, T_{cp}=14 °C for 2.0 wt.% and T_{cp}=20 °C for 2.5 wt.%. Actually, T_{cp} is higher for the studied solutions, if measured using an infinitely slow cooling rate (in a so-called equilibrium process) owing to the slow chain dynamics in this highly viscous medium. Thus, T_{cp} of the solutions, with the cellulose concentration below 2 wt.%, cannot be detected upon cooling with a 1 °C/min rate, see Figure 3. The number of chains in these solutions is small and the chains need much longer time to equilibrate below T_{cp}, *i.e*. to collapse/collide, to aggregate and to grow in size. As for 1.0 wt.% cellulose solution, clouding appear only after 2 weeks of equilibration. For comparison, turbidity formation for polystyrene in cyclohexane, below T_{cp}, can be on the order of seconds (Chu and Ying 1996).

On the other hand, T_{cp} for dilute cellulose solutions (c < 4 wt.% according to our estimation from the results presented in Figure 3) in $[P_{4444}][OAc]$:DMSO is in the low temperature range where the solvent viscosity is high and the chain dynamics are slow. Concentrated solutions (c > 4 wt.%) show T_{cp} above 40 °C, where the solvent viscosity is significantly lower, and the dynamics are faster. Figure 3 suggests the existence of a critical cellulose concentration c^*»4 wt.%. Below c^*, cooled solutions are milky, signifying the existence of large inhomogeneities/density fluctuations. Formation of particles in solutions of these concentrations is more probable. Above c^*, cooled solutions are less cloudy and transmit more light, with increasing cellulose concentration. This suggests a more homogeneous distribution of polymeric material within cold solution, which is a typical feature of homogeneous gels, or gels with inhomogeneities that are significantly smaller than the wavelength of light. It seems likely that highly

swollen semi-rigid cellulose chains strongly interact with each other at elevated temperature, above *c**. Intermolecular contacts are numerous and chains have no time to reorganize upon cooling, with the 1 °C/min rate. The slow dynamics of the phase-separation makes the chains “freeze” within the solution volume and form a physical network of interconnected chains. This network turns into a gel, which itself is a form of macroscopically phase-separated cellulose. As has been demonstrated (Callister *et al*. 1990), polystyrene forms either amorphous precipitate or gel, below the phase-separation temperature, dependent on the cooling rate and the polymer concentration.

The phase diagram of cellulose regeneration, upon cooling in $[P_{4444}][OAc]$:DMSO (70:30 w/w), is shown in Figure 4. As is seen in Figure 3, T_{cp} cannot be accurately determined for solutions of 9 wt.% and higher. The concentration of cellulose at the saturation point at 120 °C is about 13 wt.% and graphically presented with the vertical dotted line. Clear solutions (one phase) exist above the phase boundary. Probability of cellulose degradation dramatically increases above 120 °C and the horizontal dotted line shows the maximum temperature studied. Two phases exist below the phase boundary. Formation of particles is more probable below *c**, whereas, gels are likely to be formed above *c**.

Such a slow separation process cannot be detected calorimetrically, using DSC, though dissolving of MCC upon heating can be detected with DSC, see Figure S8 in SI. Analysis of the changing hydrodynamic properties of cellulose during phase-separation was initially considered using rheology. However, we anticipated that the results would not be reproducible, for particle formation, due to the shear forces applied during the measurements. The phase-separation from dilute solutions was then studied using light scattering, see Figures S9a and b in SI. An increase in the intensity of scattered light can be used to follow the initial stage of intermolecular aggregation. In order to get accurate values for the hydrodynamic diameter distributions of the particles, one needs to know solvent viscosity and refractive index. This is not a straightforward task. In spite of these difficulties, the dynamic light scattering studies demonstrated that the particles are present in the solutions when their size is too small to be detected with an optical microscope, *i.e.* below ~ 1 mm in diameter.

According to our observations, gel is readily formed at room temperature in OESs containing 30 wt.% of GVL, even if the cellulose concentration is 2 wt.%. This concentration is close to the concentration of the saturated cellulose solution, at 120 °C (see Figure 2). This means that the temperature window between the good solvation conditions and T_{cp} is practically within the experimental error. Molecules have no possibility to reorganize upon cooling. For cellulose in $[P_{4444}][OAc]$:GVL (70:30 w/w), gels remain transparent within a month, whereas cloudiness and phase-separation occur in similar solutions containing DMSO. Such differences cannot only be explained by the differences in solvent viscosities and chain mobility: viscosity of GVL is 1.86 cP at 25 °C (Kumar *et al.* 2019), whereas that of DMSO is 1.98 cP at 25 °C (Fischer Chemicals). Evidently, the differences must be dominated by the overall balance of numerous bonding interactions that exist in the cellulose-OESs.

Micro particles by regeneration from $[P_{4444}][OAc]$:DMSO (70:30 w/w)

As is demonstrated above, the cellulose concentration and the cooling conditions affect the regeneration of cellulose, in the form of micro particles or gels, when solutions are cooled below the phase-separation boundary. Regeneration in the form of particles is more probable below *c**. This leaves a very narrow window for particles formation at 20 °C (1-4 wt.%, green area in Figure 1); On one side (> 4 wt.%), gel formation occurs above *c** - on the other side (< 1 wt.%), T_{cp} is too low and chain collisions are too infrequent, resulting in too slow equilibration. Therefore, the 1-4 wt.% MCC solutions were selected to further study the regeneration to defined particles.

Two cooling procedures were tested: the slow and the fast cooling. Following our standard (slow cooling) procedure, descried in Experimental, we observed spherical particles (Figure 5) for the 2.0 wt.% solution. However, the same starting solution turns into gel if cooled down faster (fast cooling), *e.g.* by placing the solution from 120 °C directly to a fridge at 4 °C. The particles obtained using the slow cooling are uniform in size and shape, and not significantly aggregated into clusters. The diameter of the individual particles is around 30-40 μm. Higher magnification (Figure 5b) reveals that some of the particles are merged to a certain extent. The shape of the particles remains globular even when the particles stick together. This suggests that the multimolecular aggregates are formed first in the course of micro phase-separation and fuse at a later stage. In addition, it appears that the particles are also semi-crystalline spherulites since the particles exhibit a ‘Maltese cross’ in polarized light (Crist and Schultz 2016). The partial crystallization of cellulose within the particles can make their collisions elastic and enhance their colloidal stability against immediate precipitation, in addition to the high solvent viscosity. If the regeneration cycle is repeated on already regenerated cellulose (that is re-dissolution at 120 °C, followed by the slow cooling), we observe particles similar to those formed in the first cycle, which indicates that the regeneration is reversible.

Particles were also formed in the 1.0 wt.% solution. However, the regeneration was much slower in dilute solution and studied after 2 weeks of equilibration. As is shown, in Figure 6a, the size of the particles is smaller than that from the 2.0 wt.% cellulose solution (Figure 5b) even after that long equilibration. The surface of the particles is not smooth, and their shape is not as regular as that for the 2.0 wt.% solution. This can be explained by a lower collision rate in viscous medium and thus by the presence of an insufficient amount of cellulose to form well defined particles, which may result in an uneven distribution of material over the sample. Numerous repetitions demonstrate that cooling (slow cooling) of more concentrated solutions (3-4 wt.% and above) typically yielded gels, instead of particles, after 18 h equilibration: no individual particles are observed but rather inhomogeneous gel-like clusters are apparent (Figure 6b). This process is also reversible: repetition of the regeneration cycle on a gel results in formation of a gel, of a similar morphology. All this leads to a conclusion that 2.0 wt.% is an optimal concentration for the particle formation, at this solvent composition. Although, at this stage we cannot yet accurately predict similar experimental condition for another OES.

Particles are also regenerated from OESs based on $[P_{4441}][OAc]$ (Figures S1 and S2 in the SI). We used the same experimental conditions as for $[P_{4444}][OAc]$ based OESs, for comparison. However, the dissolution capacity and therefore thermodynamic quality of the $[P_{4441}][OAc]$-based OESs are in general

better than that of the analagous $[P_{4444}][OAc]$:DMSO compositions. Better thermodynamic quality also means a broader range of temperatures where MCC is soluble. One can say that $[P_{4441}][OAc]$:DMSO at RT is a 'less poor' solvent for cellulose, in comparison to $[P_{4444}][OAc]$:DMSO over the same concentration. This results in a slower phase-separation process. Accordingly, increasing the cellulose concentration promotes intermolecular interactions, increasing solution viscosity and, thus, favoring regeneration in the form of macroscopic gel. Whereas, decreasing the cellulose concentration, below 3 wt.%, improves the stability of solutions against phase-separation. This brings us to a conclusion that optimal conditions for the formation of particles from OESs based on $[P_{4441}][OAc]$ are not directly comparable with those for $[P_{4444}][OAc]$ based OESs. For this reason we did not study this system further.

Growth of regenerated particles at RT with time

Growth of the particles in $[P_{4444}][OAc]$:DMSO, within a 20 ml vial, was followed using optical microscopy. A 2.0 wt.% solution was prepared at 120 °C. It took about 30 minutes for the solution to cool down to RT and the first photos were then taken (Figure 7a). A drop of the solution was sampled from the vial to a glass slide every 30 min and the particle growth was followed over a 48 h period (Figure 7).

A clear solution with a very minor amount of micro-sized particles can be seen after the first 30 min (Figure 7a). Particles of the size smaller than one wavelength of light are already formed in this solution. This is apparent from light scattering, observed as a significant growth of scattering intensity (Figures S9a and b in SI). Bulk particles become visible under the microscope after 1.5 h (Figure 7b). The diameter of the particles is about 5-10 μm and they appear as spherulites with a nucleus in the center and vague Maltese cross pattern. Though the shape of the particles is not well-defined. The growth stops after 3.5 h, when particle sizes of 20-25 μm in diameter are reached (Figure 7c and d). The surface of the equilibrated particles is smooth, their shape is regular, and the size is uniform. They all look to be spherulites with the Maltese cross patterns.

The influence of the experimental conditions on the particle's growth was examined using another sampling method. As previously, a single drop was taken from a freshly made cellulose solution to a glass slide, after dissolution and 30 minutes equilibration at 20 °C (Figure 7a). The particle formation was followed within that drop sealed between two glass slides. The result (Figure 8) seems to differ from that when the equilibration takes place in a 20 ml vial (Figure 7c). Particles are formed and stabilized in 3.5 h using either of the methods. However, the particles that are formed in the vial are larger in size with more regular shape and structure. The contour of the particles, that grow between slides is vague and the Maltese cross patterns is less obvious.

We may conclude that the solution environment essentially affects the formation of the particles. In the method where the solution is between two slides, the space for particle diffusion is constrained and hence their collisions and growth are limited. In addition, due to the faster heat exchange that the high surface-area affords, chains of cellulose are less mobile and require much more time to crystalline within the particles, which affects their shape and polydispersity. From our extensive preliminary studies, we can

confirm that the shape and volume of the container, together with the cooling history, can significantly influence the formation of the particles. This also emphasizes the importance of standardization of the cellulose regeneration process.

Effect of non-solvent addition on regeneration of cellulose particles

It can be assumed that the addition of a non-solvent might make the thermodynamic quality of the solutions worse, which should affect the particle formation, *e.g.* possibly by making it faster. This idea is inspired by the Lyocell fiber spinning processes, where cellulose-*N*MMO-water filaments are immersed into water, causing rapid solvent exchange of *N*MMO to water and the initial stages of crystallization of cellulose (Fink *et al.* 2001). For IL-cellulose solutions, it is well know that water is an excellent non-solvent. In the approach proposed herein, small amounts of water are added to gently alter the solvent quality. This is to promote the aggregation of free chains in solution and shift the equilibrium towards the particle formation. In fiber spinning (Lyocell or IONCELL), this process Is rather rapid, ensuring a high orientation (along the fibre axis) of the cellulose chains during the regeneration process.

Several non-solvents were tested: we followed the same procedure with slow cooling to dissolve 2.0 wt.% cellulose in $[P_{4444}][OAc]$:DMSO at 120 °C (3 g in a 20 ml vial). Then the solution was stirred at 90 °C while water, acetic acid (AcOH) or ethanol (EtOH) were added in small amounts. The samples were cooled down and equilibrated at RT for 18 h before analysis using optical microscopy. The dimensions of the particles regenerated from the OES/non-solvent mixtures are shown in Table 1. The size of particles slightly increases with an increase in the non-solvent content, up to 3.0 wt.%. When the amount of the non-solvent is 5.0 wt. %, the particles become smaller again, polydisperse and with irregular shape. A small addition of non-solvent makes the particle formation less controlled with more irregular shape and size. Therefore, this does not improve the quality of the particles.

Table 1. The diameter range of the particles regenerated (slow cooling) from the 2.0 wt.% cellulose solution in presence of non-solvents and measured with an optical microscope, after 18 h of equilibration at RT.

Non-solvents	1.0 wt.%[a]	2.0 wt.% [a]	3.0 wt.% [a]	5.0 wt.%[a]
Water	10-15 µm	15-20 µm	15-20 µm	10-20 µm
AcOH	10-15 µm	20-30 µm	20-30 µm	7-15 µm
EtOH	15-30 µm	15-30 µm	20-35 µm	10-30 µm

[a] *wt.% of non-solvent in the OES-cellulose mixture*.

Preparation of dry particles

Thinking of a possible application for cellulose, in the form of individual and well-defined micro particles, we attempted extraction of the already formed particles from the OES. To extract the particles from the

[P_{4444}][OAc]:DMSO solutions, a rapid solvent exchange was applied to wash the OESs away: 10 times larger weight of non-solvents (water, acetone, ethanol, acetonitrile, formamide and pyridine) were added into the regenerated cellulose solutions (all 2.0 wt.% after slow cooling to RT and then equilibrated at RT for 18 h).

If and when water was added, the dispersions of the particles became less opaque but no obvious precipitation of cellulose was detected. Probe sonication was applied to the cellulose-OES solution and water mixture, which was efficient enough to prevent formation of large agglomerates. After sonication, the particles were recovered by centrifugation (typically over 20 min at 3000 rpm). Further washing and centrifugation of the sedimented particles with water was repeated 3 times.

To examine if there was any IL residue in the product, tiny amount of the product was mixed with DMSO-d_6 (about 0.2 wt.%) and heated at 100 °C for 1 h, with magnetic stirring. DMSO does not dissolve cellulose. Although, if there is any IL residue the heating helps to extract IL from the dried particles and the IL signals can easily be observed. No IL residue has been detected indicating the washing was successful.

Figure 9 shows particles in OES and in pure water after washing. The surface of the redispersed particles (Figure 9b) is more defined in water and the shape remains spherical. However, the Maltese Cross pattern is not observed. This may be because the surface of the cellulose particles is coated with a water “shell” that makes the Maltese Cross invisible, or it may be related to extraction of the IL from the existing crystalline phase, increasing disorder in the system. The particles also look like they may have shrunk a little, as the surface looks more wrinkled. This would be consistent with some kind of volume change upon recrystallisation, as the IL is removed. The estimated yield of the transferred cellulose (dry product) from OES to water is ~ 90 %. If the particles are already merged in OES into multi particles clusters, they remain clustered during the washing with water, which calls for further optimization of the conditions for recovery of defined particles and size distributions.

Washing with acetone differs from washing with water. The dispersions of particles in the acetone/OES mixtures first become cloudier with precipitation but then clarify during 20 min of sonication. Seemingly, the sonication breaks the particles and their clusters into smaller pieces that are too small to be detected by microscope. Sedimentation of these nano-scale particles with a centrifuge is not possible. Therefore, dynamic light scattering was used for detecting these particles in the acetone/OES mixtures after sonication. Because of the great excess of acetone in the mixture, we used the viscosity and the refractive index of acetone to roughly estimate the mean hydrodynamic diameter of the particles as 150 nm, see Figures S10 and S11 in SI. This requires further study as novel morphologies of nanocellulose may be possible.

Addition of ethanol, acetonitrile and formamide to the cellulose-OES dispersions result in strong inter particles association, in the form of large fiber-like flocs. In pyridine, the particles swell to a certain extent

and loss their structure. The addition of small amounts of these solvents may temporarily allow for swelling and redissolution of cellulose, until bulk regeneration.

Wide angle X-ray scattering (WAXS) of final product

Dry particles extracted from the acetone/OES mixture were examined by means of wide angle X-ray scattering (WAXS) in Brent-Brentano geometry from a pressed pellet of the particles. Figure 10 shows the result obtained from WAXS (orange line), which is typical the Cellulose II 1D diffraction pattern (French 2014; Langan *et al.* 2001). The diffraction pattern also contains a significant amorphous contribution The crystallinity of cellulose II is 37.2%, which has been calculated based on the method of Rico del Cerro, D., *et al* (Rico del Cerro *et al.* 2020). The peak fitting is shown in Figure S12 (SI).

The WAXS results support the results obtained using microscopy: the particles are crystalline, which is evident from their spherulitic nature. Cellulose chains firstly form highly ordered lamellae, with antiparallel motifs (consistent with cellulose II). The lamellae are then connected by amorphous region. In other polymer systems, the Maltese cross is caused by the alignment though highly ordered lamella (Carraher 2003). What is not clear is, how much the cellulose II crystallinity comes from regeneration of the particles and how much comes from crystallization of free cellulose chains, during the washing stage. However, considering that bulk gelation was not observed, we believe that only a very small fraction of the cellulose chains remained in the solution, prior to non-solvent washing.

Conclusions

The solutions of cellulose in the $[P_{4444}][OAc]$:DMSO mixtures undergo a phase separation upon cooling. The phenomenon resembles the upper critical solution temperature (UCST) behavior known for synthetic polymers. This behavior does not seem to be specific for the studied system and may be a general phenomenon for cellulose-OES compositions (Clough et al. 2017; de Oliveira et al. 2016; Holding et al. 2017).

This work is one of the first attempts to perform a detailed mechanistic study on the UCST-type transition of cellulose. A phase separation diagram was constructed by measuring the cloud point temperature (T_{cp}). Depending on the experimental conditions, cellulose regenerates in the form of individual spherical particles/aggregates, multi particles clusters or macroscopic gels.

This phase preparation phenomena was used to prepare cellulose particles with highly ordered shape and size. In these systems, the regeneration process is a consequence of multi-parameter interdependence, e.g., cellulose concentration, solvent composition, cooling rate, and time of equilibration. Regular particles are only formed in a rather narrow window of the phase diagram. At RT, ordered particles are reproducibly regenerated with 1-2 wt.% cellulose in $[P_{4444}][OAc]$:DMSO (70:30 w/w). However, the solutions turn into gel upon cooling at higher cellulose concentrations, whereas, micro-sized particles can barely form at more dilute concentrations.

The thermodynamic quality of the cellulose solutions in $[P_{4444}][OAc]$:DMSO is poor below the T_{cp} and individual cellulose chains start to aggregate with time and form the particles. Due to the high viscosity of the OES at the lower temperatures, the motion of the cellulose chains becomes slower, which favors gradual growth and crystallization of the cellulose within the particles. If the cooling rate is too fast, or the concentration is too high, the high solvent viscosity makes the still swollen chains 'freeze' in position within the solution volume and form physical network, which leads to the formation of macroscopic gel below T_{cp}. While the regeneration phenomena can be easily visualized by optical microscopy, understanding the principles of these processes are necessary to enable control over the size and shape of the regenerated particles. Thus, careful tuning of the solvent composition, cellulose concentration and cooling profile are required.

The colloidal stability of multi molecular particles formed by synthetic polymers in poor solvents may be explained by the viscoelastic effect or/and by the partial vitrification of polymeric material (Aseyev et al. 2006; Zhang and Wu 2006). Evidently, partial crystallization of cellulose within the particles can make their collisions elastic and enhance their colloidal stability against immediate precipitation, in addition to the high solvent viscosity.

Highly regular micro-sized particles were regenerated from the optimum $[P_{4444}][OAc]$:DMSO mixture, using water as an additive/non-solvent. The freeze-dried particles are composed of cellulose II (37.2%) and amorphous cellulose. However, in this preliminary work, the obtained particles were clustered to a certain extent during the washing process, indicating their soft nature and tendency for aggregation.

The UCST-type behavior of cellulose solutions in OES's offers a tempting approach to regenerate dissolved cellulose into well-defined, regular particles. Though the phase separation phenomena has previously been observed for other cellulose solvents, isolation of the particles in a solvent free form has not been demonstrated.

Declarations

Acknowledgements

Financial support of the Academy of Finland (Code: 310481) and Business Finland (Valcel) are gratefully acknowledged.

References

Andanson J-M, Bordes E, Devémy J, Leroux F, Pádua AAH, Gomes MFC (2014) Understanding the role of co-solvents in the dissolution of cellulose in ionic liquids. Green Chem 16:2528-2538. https://doi.org/10.1039/C3GC42244E

Arnauts J, Berghmans HJPc (1987) Amorphous thermoreversible gebs of atadic polystyrene. Polym Commun (Guildford) 28:66-68

Aseyev VO, Tenhu H, Winnik FM (2006) Temperature dependence of the colloidal stability of neutral amphiphilic polymers in water. Conformation-dependent design of sequences in copolymers II. Springer, pp 1-85

Bradaric CJ, Downard A, Kennedy C, Robertson AJ, Zhou Y (2003) Industrial preparation of phosphonium ionic liquids. Green Chem 5:143-152. https://doi.org/10.1039/B209734F

Callister S, Keller A, Hikmet RM (1990) On thermoreversible gels: their classification, relation to phase transitions and vitrification, their morphology and properties. Makromol Chem, Macromol Symp 39: 19-54. https://doi.org/10.1002/masy.19900390104

Carraher CE (2003) Seymour/Carraher's polymer chemistry: Sixth Edition. CRC Press, pp 44-45

Chu B, Ying Q (1996) Single-chain expansion from the collapsed globule of polystyrene in cyclohexane to the Θ coil. Macromolecules 29:1824-1826. https://doi.org/10.1021/ma951089+

Clough MT (2017) Organic electrolyte solutions as versatile media for the dissolution and regeneration of cellulose. Green Chem 19:4754-4768. https://doi.org/10.1039/c7gc01776f

Clough MT, Fares C, Rinaldi R (2017) 1D and 2D NMR spectroscopy of bonding interactions within stable and phase-separating organic electrolyte-cellulose solutions. ChemSusChem 10:3452-3458. https://doi.org/10.1002/cssc.201701042

Crist B, Schultz JM (2016) Polymer spherulites: A critical review. Prog Polym Sci 56:1-63 https://doi.org/10.1016/j.progpolymsci.2015.11.006

de Oliveira HF, Clough MT, Rinaldi R (2016) Thermally triggered phase-separation of organic electrolyte-cellulose solutions. ChemSusChem 9:3324-3329. https://doi.org/10.1002/cssc.201601108

Dupont A-L, Tetreault J (2000) Cellulose degradation in an acetic acid environment. Stud Conserv 45:201-210. https://doi.org/10.1179/sic.2000.45.3.201

Elsayed S, Hellsten S, Guizani C, Witos J, Rissanen M, Rantamäki AH, Varis P, Wiedmer SK, Sixta H (2020a) Recycling of superbase-based ionic liquid solvents for the production of textile-grade regenerated cellulose fibers in the Lyocell process. ACS Sustainable Chem Eng 8: 14217–14227. https://doi.org/10.1021/acssuschemeng.0c05330

Elsayed S, Viard B, Guizani C, Hellsten S, Witos J, Sixta H (2020b) Limitations of cellulose dissolution and fiber spinning in the Lyocell process using [mTBDH][OAc] and [DBNH][OAc] solvents. Ind Eng Chem Res 59:20211-20220. https://doi.org/10.1021/acs.iecr.0c04283

Fink H-P, Weigel P, Purz H, Ganster J (2001) Structure formation of regenerated cellulose materials from NMMO-solutions. Prog Polym Sci 26:1473-1524. https://doi.org/10.1016/S0079-6700(01)00025-9

French AD (2014) Idealized powder diffraction patterns for cellulose polymorphs. Cellulose 21:885-896. https://doi:10.1007/s10570-013-0030-4

Ge S, Zhang L, Zhang Y, Lan F, Yan M, Yu JJN (2017) Nanomaterials-modified cellulose paper as a platform for biosensing applications. Nanoscale 9:4366-4382. https://doi.org/10.1039/C6NR08846E

Gong J, Li J, Xu J, Xiang Z, Mo L (2017) Research on cellulose nanocrystals produced from cellulose sources with various polymorphs. RSC Adv 7:33486-33493. https://doi.org/10.1039/C7RA06222B

Hanke CG, Atamas NA, Lynden-Bell RM (2002) Solvation of small molecules in imidazolium ionic liquids: a simulation study. Green Chem 4:107-111. https://doi.org/10.1039/B109179B

Hauru LK, Hummel M, Nieminen K, Michud A, Sixta H (2016) Cellulose regeneration and spinnability from ionic liquids. Soft Matter 12:1487-1495. https://doi.org/10.1039/c5sm02618k

Himmel ME, Ding S-Y, Johnson DK, Adney WS, Nimlos MR, Brady JW, Foust TD (2007) Biomass recalcitrance: engineering plants and enzymes for biofuels production. Science 315:804-807. https://doi.org//10.1126/science.1137016

Holding AJ (2016) Ionic liquids and electrolytes for cellulose dissolution. Dissertation, University of Helsinki

Holding AJ, Heikkila M, Kilpelainen I, King AW (2014) Amphiphilic and phase-separable ionic liquids for biomass processing. ChemSusChem 7:1422-1434. https://doi.org/10.1002/cssc.201301261

Holding AJ, Parviainen A, Kilpeläinen I, Soto A, King AWT, Rodríguez H (2017) Efficiency of hydrophobic phosphonium ionic liquids and DMSO as recyclable cellulose dissolution and regeneration media. RSC Adv 7:17451-17461. https://doi.org/10.1039/C7RA01662J

Huo F, Liu Z, Wang W (2013) Cosolvent or antisolvent? A molecular view of the interface betweenionic liquids and cellulose upon addition of another molecular solvent. J Phys Chem B 117:11780-11792. http://doi.org/10.1021/jp407480b

Ingildeev D, Effenberger F, Bredereck K, Hermanutz F (2013) Comparison of direct solvents for regenerated cellulosic fibers via the lyocell process and by means of ionic liquids. J Appl Polym Sci 128:4141-4150. https://doi.org/10.1002/app.38470

King AW, Asikkala J, Mutikainen I, Järvi P, Kilpeläinen I (2011) Distillable acid–base conjugate ionic liquids for cellulose dissolution and processing. Angew Chem, Int Ed 50:6301-6305. https://doi.org/10.1002/anie.201100274

King AWT, Mäkelä V, Kedzior SA, Laaksonen T, Partl GJ, Heikkinen S, Koskela H, Heikkinen HA, Holding A J, Cranston E D, Kilpeläinen I (2018) Liquid-state NMR analysis of nanocelluloses. Biomacromolecules 19:2708-2720. http://doi.org/10.1021/acs.biomac.8b00295

King AWT, Parviainen A, Karhunen P, Matikainen J, Hauru LKJ, Sixta H, Kilpeläinen I (2012) Relative and inherent reactivities of imidazolium-based ionic liquids: the implications for lignocellulose processing applications. RSC Adv 2:8020-8026. https: //doi.org/10.1039/C2RA21287K

Koso T, Rico del Cerro D, Heikkinen Si, Nypelö T, Buffiere J, Pe-Buceta JE, Potthast A, Rosenau T, Heikkinen H, Maaheimo H, Isogai A, Kilpeläinen I, King AWT (2020) 2D Assignment and quantitative analysis of cellulose and oxidized celluloses using solution-state NMR spectroscopy. Cellulose 27:7929-7953. http://doi.org/10.1007/s10570-020-03317-0

Kumar A, Sharma A, de la Torre BG, Albericio F (2019) Scope and limitations of γ-valerolactone (GVL) as a green solvent to be used with base forfmoc removal in solid phase peptide synthesis. Molecules 24:4004. https://doi.org/10.3390/molecules24214004

Langan P, Nishiyama Y, Chanzy H (2001) X-ray structure of mercerized cellulose II at 1 Å resolution. Biomacromolecules 2:410-416. https://doi.org/doi:10.1021/bm005612q

Lopez J, Pletscher S, Aemissegger A, Bucher C, Gallou F (2018) N-butylpyrrolidinone as alternative solvent for solid-phase peptide synthesis. Org Process Res Dev 22:494-503. https://doi.org/10.1021/acs.oprd.7b00389

Mikkola, S-K, Robciuc A, Lokajova J, Holding AJ, Laemmerhofer M, Kilpelainen I, Holopainen JM, King AW T & Wiedmer SK (2015) Impact of amphiphilic biomass-dissolving ionic liquids on biological cells and liposomes. Environ Sci Technol 49:1870-1878. https://doi.org/10.1021/es505725g

Nishiyama Y, Sugiyama J, Chanzy H, Langan P (2003) Crystal structure and hydrogen bonding system in cellulose Iα from synchrotron X-ray and neutron fiber diffraction. J Am Chem Soc 125:14300-14306. https://doi.org/10.1021/ja037055w

Parviainen A, King AWT, Mutikainen I, Hummel M, Selg C, Hauru LKJ, Sixta H & Kilpeläinen I (2013) Predicting cellulose solvating capabilities of acid-base conjugate ionic liquids. ChemSusChem 6:2161-2169. https://doi.org/10.1002/cssc.201300143

Rabideau BD, Agarwal A, Ismail AE (2013) Observed mechanism for the breakup of small bundles of cellulose Iα and Iβ in ionic liquids from molecular dynamics simulations. J Phys Chem B 117:3469-3479. https://doi.org/10.1021/jp310225t

Rabideau BD, Agarwal A, Ismail AE (2014) The role of the cation in the solvation of cellulose by imidazolium-based ionic liquids. J Phys Chem B 118:1621-1629. https://doi.org/10.1021/jp4115755

Rico del Cerro D, Koso TV, Kakko T, King AWT, Kilpeläinen I (2020) Crystallinity reduction and enhancement in the chemical reactivity of cellulose by non-dissolving pre-treatment with tetrabutylphosphonium acetate. Cellulose 27:5545-5562. https://doi.org/10.1007/s10570-020-03044-6

Rinaldi R (2011) Instantaneous dissolution of cellulose in organic electrolyte solutions. Chem Commun 47:511-513. https://doi.org/10.1039/C0CC02421J

Roy P, Roy U, Dube DK, (1984) Immobilised cellulolytic and hemicellulolytic enzymes from Macrophomina phaseolina. J Chem Technol Biotechnol 34:165-170. https://doi.org/10.1002/jctb.280340304

Schrems M, Ebner G, Liebner F, Becker E, Potthast A, Rosenau T (2010) Side reactions in the system cellulose/1-alkyl-3-methyl-imidazolium ionic liquid. ACS Symp Ser 1033:149-164. https://doi.org/10.1021/bk-2010-1033.ch008

Sixta H, Michud A, Hauru L, Asaadi S, Ma Y, King AWT, Kilpeläinen I & Hummel M (2015) Ioncell-F: A High-strength regenerated cellulose fibre. Nord Pulp Pap Res J 30:43-57. https://doi.org/10.3183/npprj-2015-30-01-p043-057

Song G, Yu J, Ding M, Zhang J (2018) A Novel Cellulose/Ionic Liquid Complex Crystal. Cryst Growth Des 18:4260-4264. https://doi.org/10.1021/acs.cgd.8b00754

Song H, Niu Y, Yu J, Zhang J, Wang Z, He J (2013) Preparation and morphology of different types of cellulose spherulites from concentrated cellulose ionic liquid solutions. Soft Matter 9:3013-3020. https://doi.org/10.1039/c3sm27320b

Stepanek P, Konak C, Sedlacek B (1982) Coil-globule transition of a single polystyrene chain in dioctyl phthalate. Macromolecules 15:1214-1216. https://doi.org/10.1021/ma00232a056

Stoppa A, Hunger J, Buchner R (2009) Conductivities of binary mixtures of ionic liquids with polar solvents. J Chem Eng Data 54:472-479. https://doi.org/10.1021/je800468h

Sun ST, Nishio I, Swislow G, Tanaka T (1980) The coil–globule transition: Radius of gyration of polystyrene in cyclohexane. J Chem Phys 73:5971-5975. https://doi.org/10.1063/1.440156

Swatloski RP, Spear SK, Holbrey JD, Rogers RD (2002) Dissolution of cellose with ionic liquids. J Am Chem Soc 124:4974-4975. https://doi.org/10.1021/ja025790m

Swislow G, Sun S-T, Nishio I, Tanaka T (1980) Coil-globule phase transition in a single polystyrene chain in cyclohexane. Phys Rev Lett 44:796-798. https://doi.org/10.1103/PhysRevLett.44.796

Terinte N, Ibbett R, Schuster K (2011) Overview on native cellulose and microcrystalline cellulose I structure studied by X-ray diffraction (WAXD): Comparison between measurement techniques. Lenzinger Ber 89:118-131

Ullah H, Santos HA, Khan T (2016) Applications of bacterial cellulose in food, cosmetics and drug delivery. Cellulose 23:2291-2314. https://doi.org/110.1007/s10570-016-0986-y

Willcock H, Lu A, Hansell CF, Chapman E, Collins IR, O'Reilly RK (2014) One-pot synthesis of responsive sulfobetaine nanoparticles by RAFT polymerisation: the effect of branching on the UCST cloud point. Polym Chem 5:1023-1030. https://doi.org/10.1039/C3PY00998J

Wojdyr MJJoac (2010) Fityk: a general-purpose peak fitting program. J Appl Crystallogr 43:1126-1128. https://doi.org/10.1107/S0021889810030499

Zhang G, Wu C (2006) Folding and formation of mesoglobules in dilute copolymer solutions. Conformation-dependent Design of Sequences in copolymers I. Springer, pp 101-176

Figures

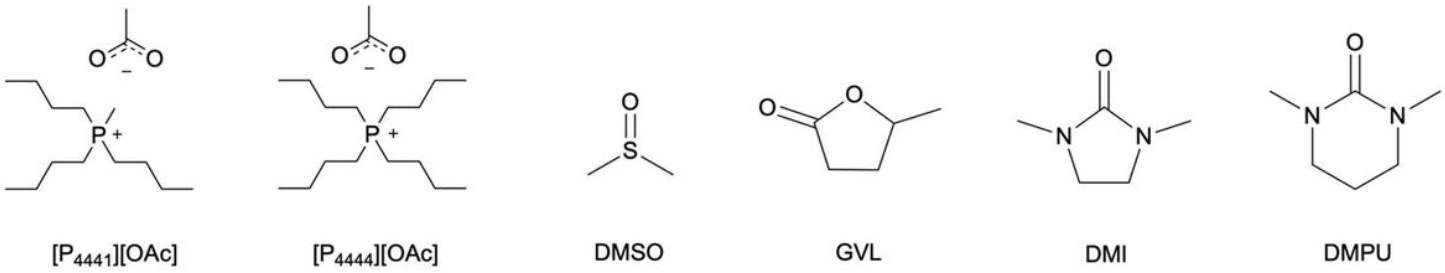

Figure 1

Chemical structures of the studied ionic liquids (ILs) and co-solvents.

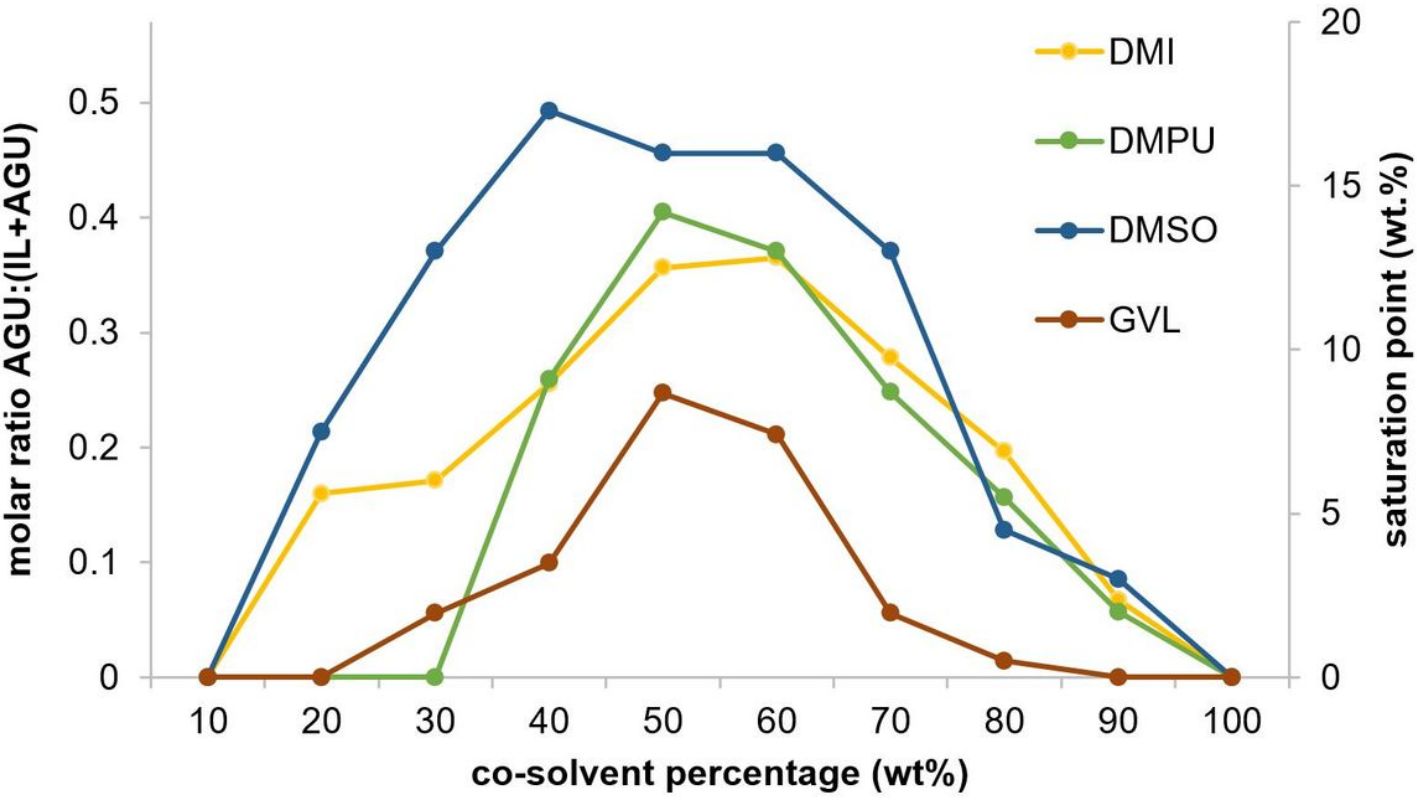

Figure 2

Dissolution capacity of binary OESs containing [P4444][OAc] as IL and various co-solvents determined as concentration of cellulose in its saturated solutions at 120 °C.

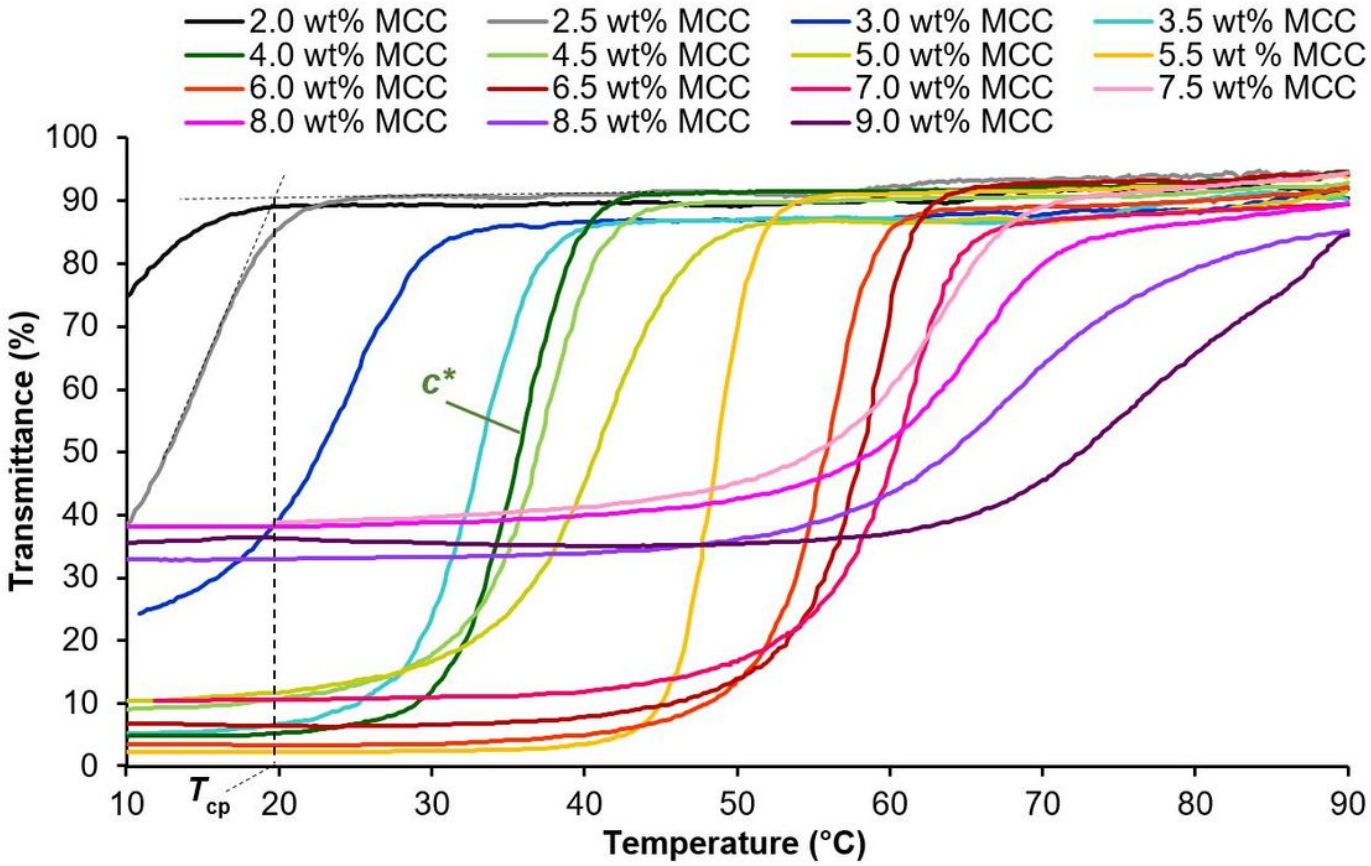

Figure 3

Change in turbidity of cellulose in [P4444][OAc]:DMSO (70:30 w/w) upon cooling with a constant 1 °C/min cooling rate. Example of the Tcp determination for the 2.5 wt.% solution is shown with dotted lines.

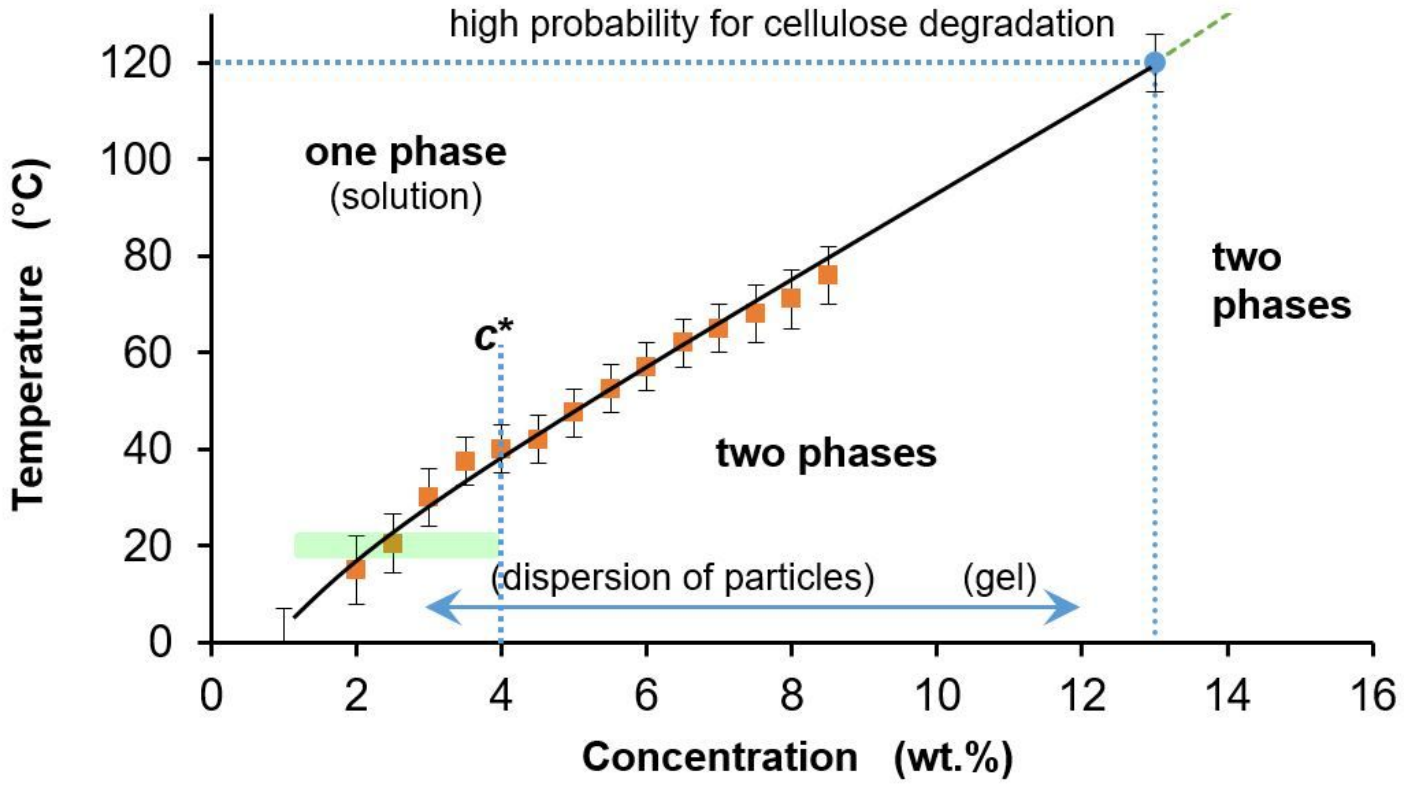

Figure 4

The phase diagram of cellulose in [P4444][OAc]:DMSO (70:30 w/w). Green area shows the concentration range where the regeneration of cellulose, in the form of particles, at 20 °C is the most probable.

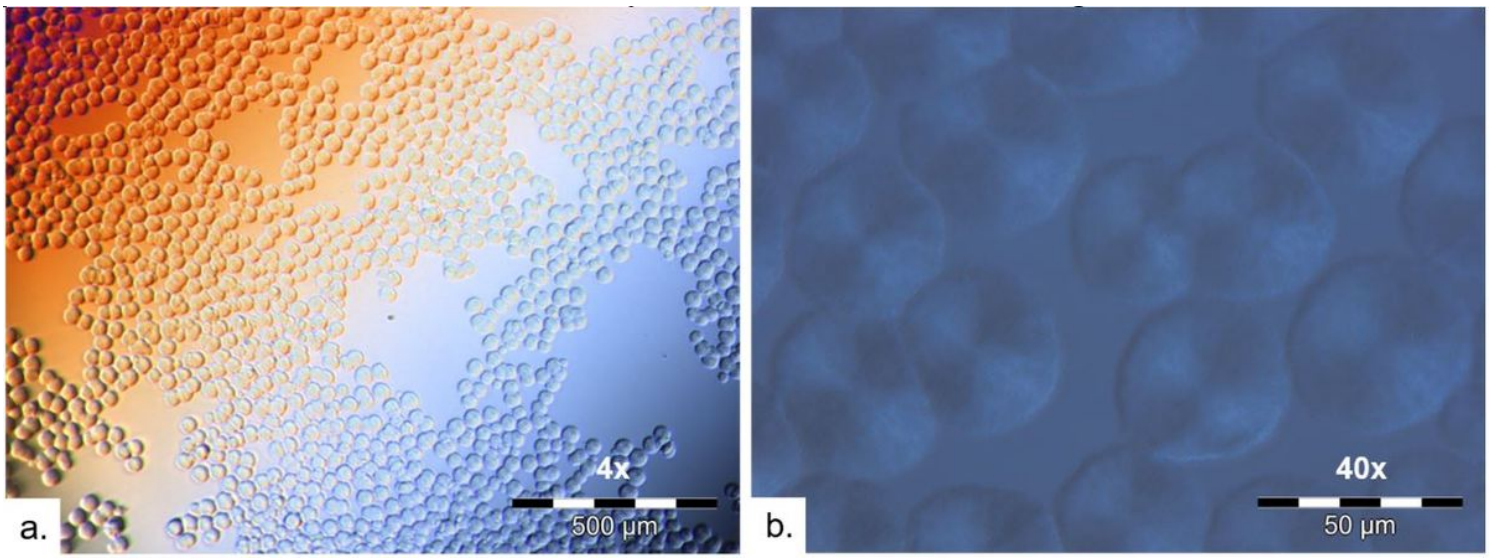

Figure 5

Regenerated cellulose particles visualized with 4x (a) and 40x (b) magnifications in 2.0 wt.% cellulose solution in [P4444][OAc]:DMSO. Particles are obtained upon slow cooling and equilibration at RT for 18 h.

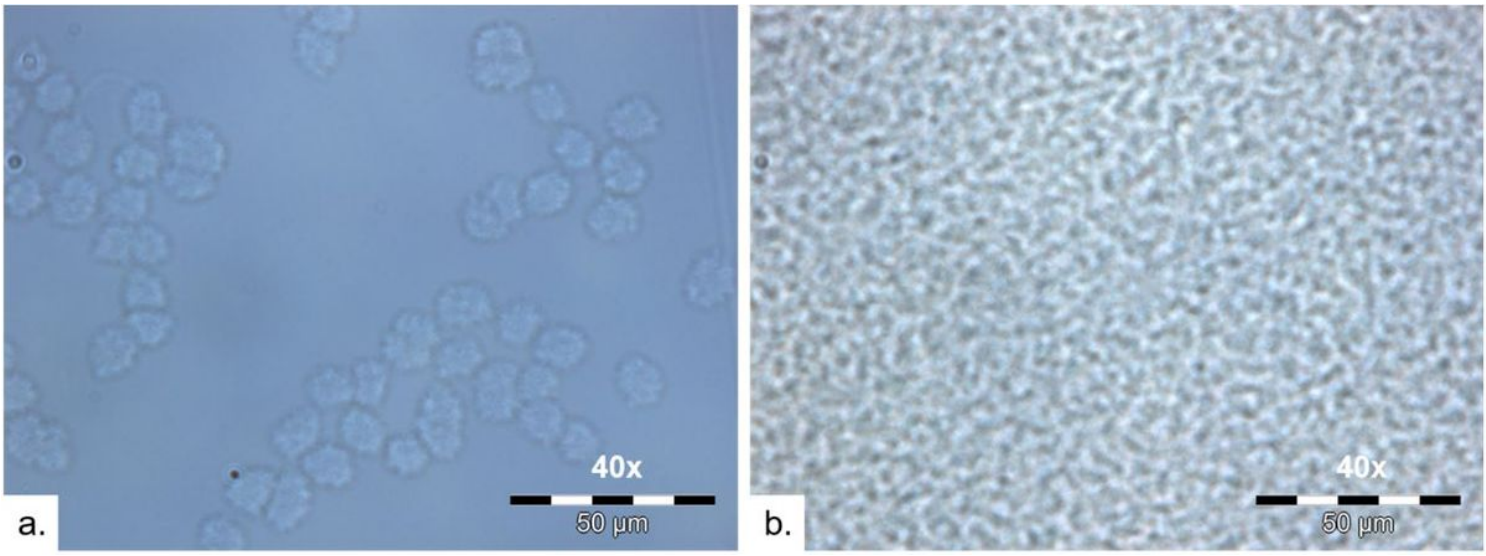

Figure 6

Regenerated cellulose from 1.0 (a) and 3.0 (b) wt.% solutions after slow cooling and equilibrating at RT. The equilibration time for 1.0 wt.% solution is 2 weeks and for 3.0 wt.% is 18 h.

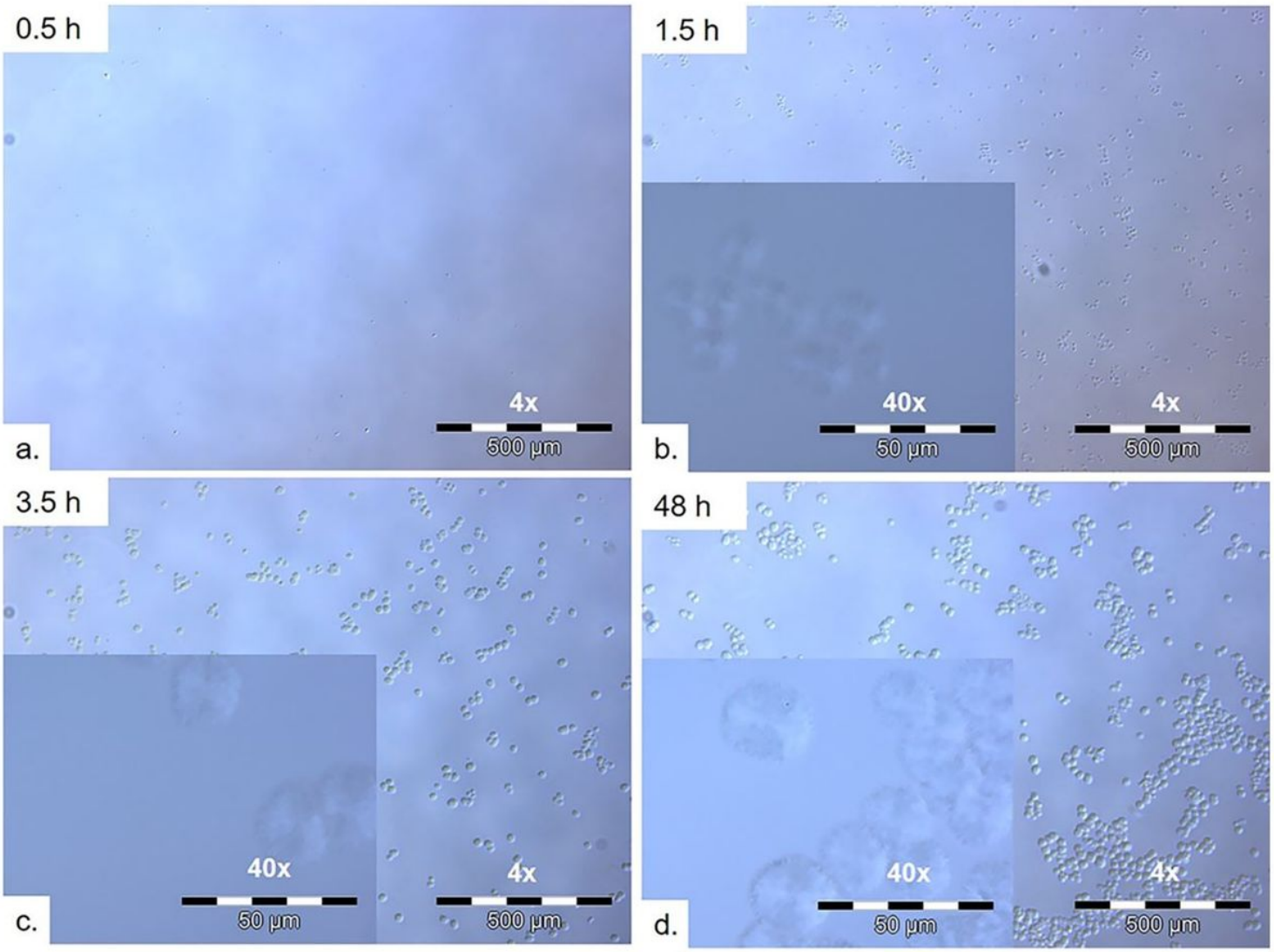

Figure 7

Process of the particles formation in 2.0 wt.% [P4444][OAc]:DMSO inside a 20 ml vial after slow cooling with increasing equilibration time at RT.

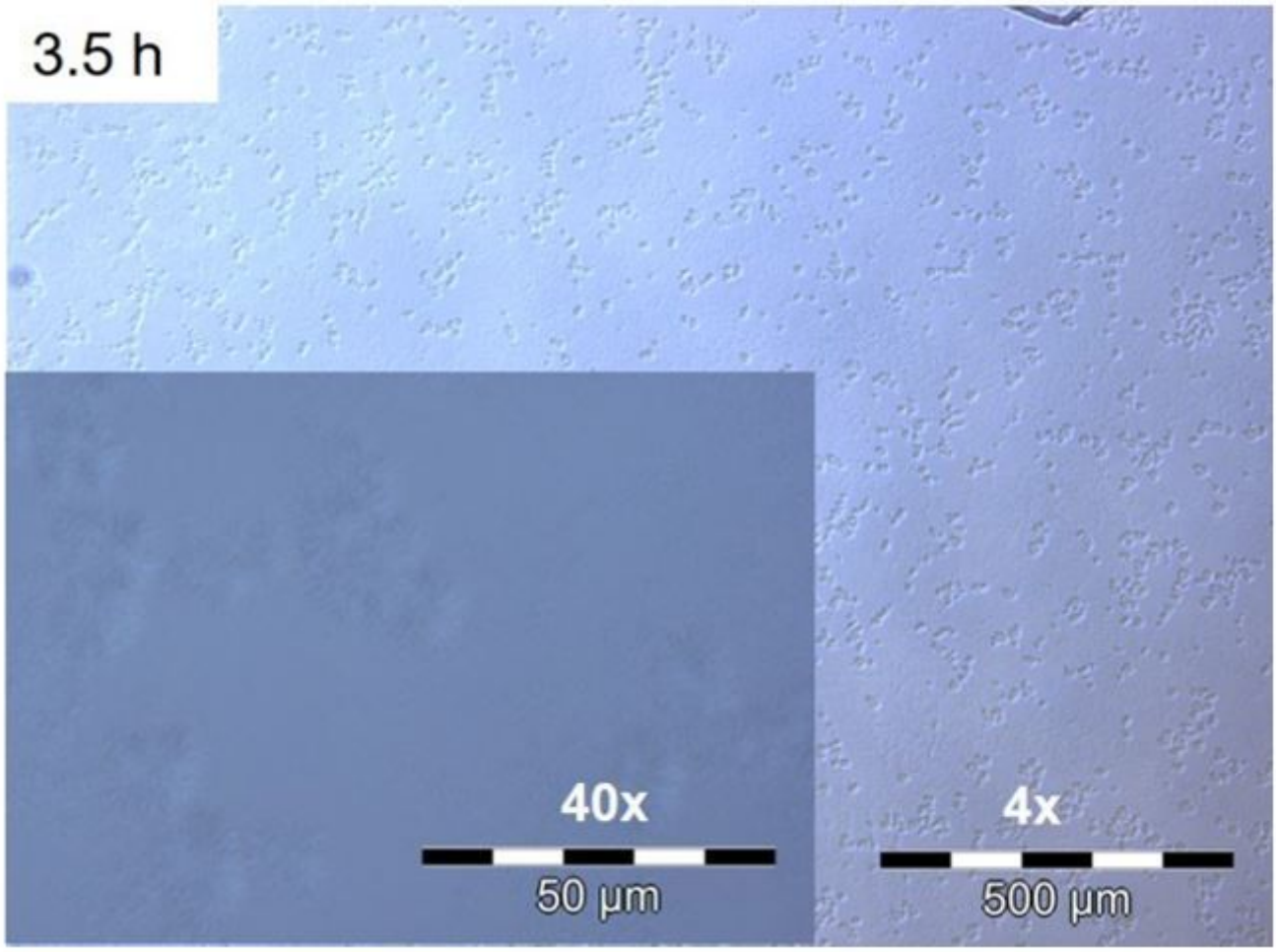

Figure 8

The result of the particles formation between two glass slides in 2.0 wt.% [P4444][OAc]:DMSO with slow cooling to RT after 3.5 h.

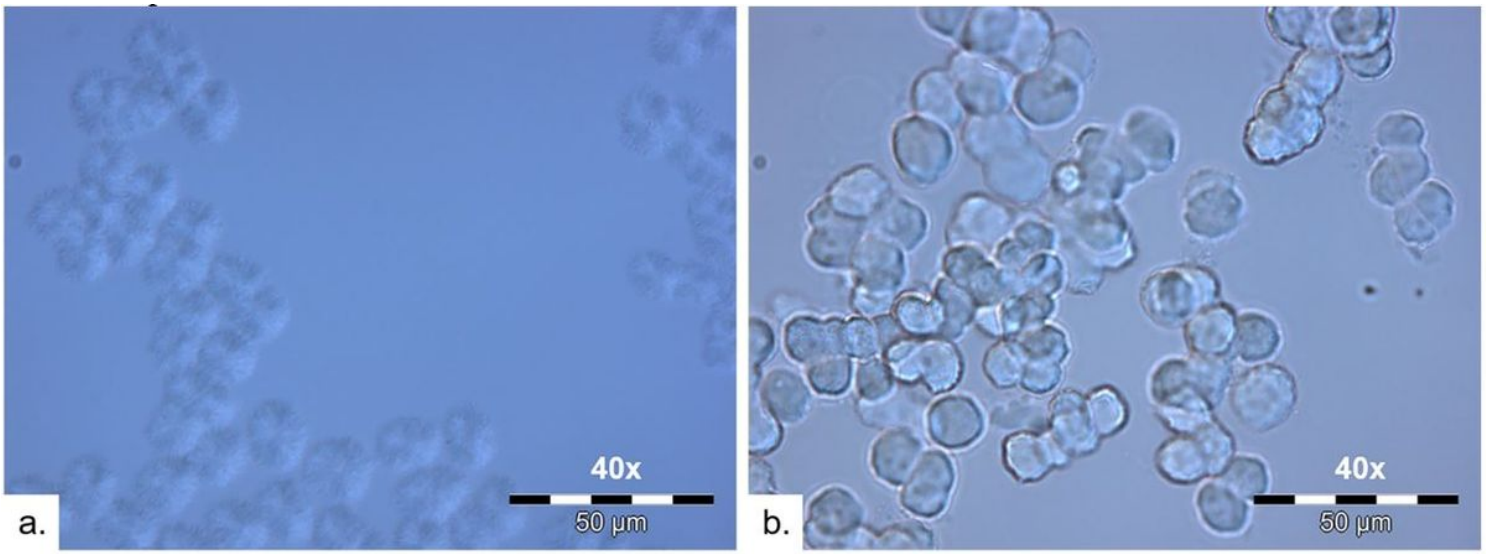

Figure 9

Regenerated particles from 2.0 wt.% solutions in [P4444][OAc]:DMSO (70:30 w/w) with slow cooling to RT and 18 h equilibration (a) and the particles washed and redispersed in water (b).

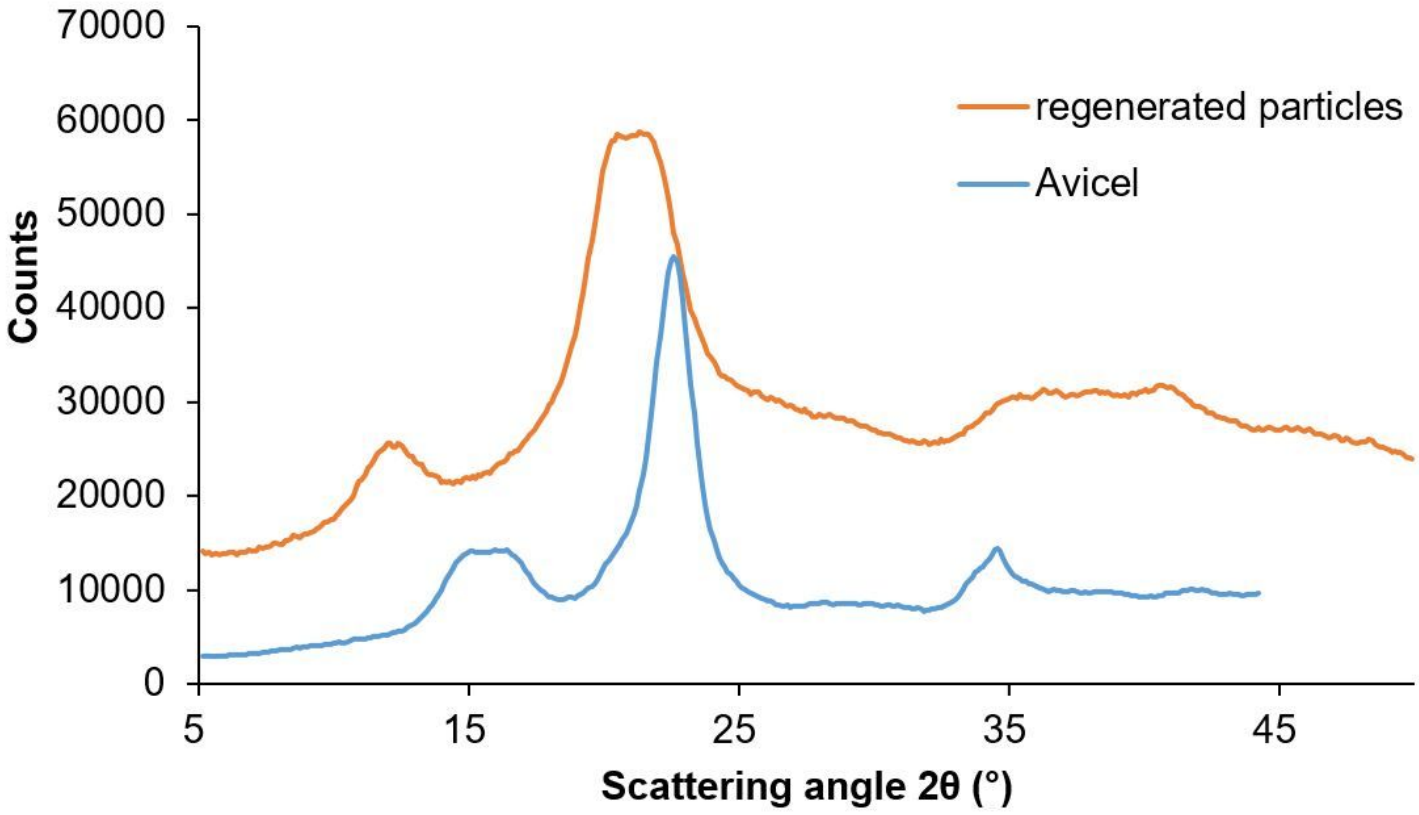

Figure 10

Wide angle X-ray scattering representing freeze dried regenerated cellulose in the form of particles and original MCC (Avicel).

Supplementary Files

This is a list of supplementary files associated with this preprint. Click to download.

- graphicsabstract.jpg
- Fig.S2.tif
- Fig.S3.tif
- Fig.S4.tif
- Fig.S5.tif
- Fig.S6.tif
- Fig.S7.tif
- Supplinfofinal1404202JX.docx